TIM-21-03533

# Thermally modulated CMOS compatible particle sensor for air quality monitoring

Jan Peter Specht, Siavash Esfahani, Yuxin Xing, Anton Köck, Marina Cole, Julian William Gardner, *Fellow, IEEE*

***Abstract*—Combating the health effects of particulate matter pollution requires affordable and reliable real-time air quality monitoring. The potential for large-scale manufacturing of acoustic wave-based sensors makes them an interesting option for low-cost, low-power particle sensing applications. This paper demonstrates a solidly mounted resonator particulate matter sensor with improved sensitivity through thermal modulation of the device. A novel, CMOS compatible solidly mounted resonator with an integrated microheater was designed, manufactured, and tested. In simulations, it was found that particle deposition increases both the heat loss and the thermal time constant of the solidly mounted resonator. The effect of this on the resonant frequency shift of the device caused by particle deposition is investigated closely in this work. The sensitivity of the devices to particle deposition was tested experimentally with and without temperature modulation by placing the device in a test chamber and allowing the randomised settling of aerosolised particles on its surface. The unmodulated sensor demonstrated a particle mass sensitivity of ~ 40 Hz/ng whilst the mass sensitivity of the temperature-modulated device was shown to improve by a factor of nearly × 5 to 190 Hz/ng. Temperature modulation also improved the detection limit from 100 ng to 50 ng. Further experiments were conducted by adding an impactor mechanism to have a more controlled measurement set up. To this effect a thermophoretic particle deposition mechanism was added to the device to enhance its performance. It was demonstrated that the repeatability of measurements was significantly improved, making the device a promising low-cost technology for air quality monitoring.**

***Index Terms*—Air quality measurement, particle sensor, bulk acoustic wave resonator, solidly mounted resonator, temperature modulation, thermophoresis.**

## I. Introduction

THE effect of air pollution on the human respiratory system is of increasing concern. Human exposure to air pollution has been linked to increased rates of COVID-19 mortality [1]. A link between COVID-19 cases and concentration of airborne particulate matter (PM) at regional level was reported in [2] and [3]. Particulate matter emission sources are both anthropogenic and natural. PM encompasses, for example, particles of sulphate, black carbon or dust from erosion and pollen [4], [5]. Particles are generally classified by diameter, with ultrafine, 2.5 µm (PM2.5) and 10 µm (PM10) being of the most interest [4], [5] in terms of air pollution. A policy assessment published by the United States Environmental Protection Agency (US EPA) also assumes a causal relation between human exposure to particulate matter pollution and cardiovascular effects and mortality [4]. To reduce the number of premature deaths caused by exposure to particulate matter, governments worldwide have defined standards for particulate matter concentrations [6]. It has been found that pollution limits imposed over smaller timescales can lead to increased health benefits. The effect of these regulations is currently limited by the extent to which localised, real-time pollution data is available [4]. To improve this, it is necessary to develop inexpensive, low-power, readily available equipment for real-time particulate matter measurement [5], [7]–[10]. This would especially help to increase spatial resolution of pollution data [5], [9]. Equipment that is less expensive and less bulky would also help the development of personal air quality monitoring instrumentation [5], [11]. Both the development of a novel, inexpensive particle sensor and a novel method to improve its capability are presented in this paper.

Currently, the US EPA Air Quality System (AQS), approves PM2.5 or PM10 concentration measurement devices using gravimetric, beta attenuation monitors or optical methods [12], [13]. The working principle of these methods, as well as their main advantages and disadvantages are listed in Table I. The main drawback of these methods is their high-power consumption and large volume, as well as their relatively high cost.

Gravimetric particle sensors based on piezoelectric microelectromechanical systems (MEMS) attempt to resolve the highlighted issues [8], [14]–[21]. Gravimetric MEMS sensors commonly rely on measuring the change in resonant frequency caused by particles settling on the sensing area. The frequency shift is caused by the resulting change in the mass and the thickness of the sensing area [22]. Resonant cantilever sensors, for example, are simple and inexpensive to manufacture. They have been shown to be capable of particle

This paragraph of the first footnote will contain the date on which you submitted your paper for review, which is populated by IEEE. “This work was supported in part by financial support under the scope of the COMET program within the K2 Centre “Integrated Computational Material, Process and Product Engineering (IC-MPPE)” (Project No 859480). This program is supported by the Austrian Federal Ministries for Transport, Innovation and Technology (BMVIT) and for Digital and Economic Affairs (BMDW), represented by the Austrian research funding association (FFG), and the federal states of Styria, Upper Austria, and Tyrol. *(Corresponding author: J. W. Gardner).*

Jan Peter Specht, Siavash Esfahani, Yuxin Xing, Marina Cole, and Julian William Gardner are with the Microsensors and Bioelectronics Laboratory, School of Engineering, University of Warwick, Coventry CV4 7AL, U.K. (e-mail: j.w.gardner@warwick.ac.uk).

Anton Köck is with the Materials Center Leoben Forschung GmbH (MCL), 8700 Leoben, Austria.

Color versions of one or more of the figures in this article are available online at http://ieeexplore.ieee.org

TABLE I.
PARTICLE MONITORING METHODS

| Method | Working Principle | Advantages | Drawbacks |
|---|---|---|---|
| Particle Sampler (gravimetric) | Fan passes polluted air through a filter that captures the particles [5]. Particle concentration is calculated from volumetric air flow rate and the change in mass of the particle filter | - Accurate for long measurement intervals [13]<br>- Widely used [12], [13] | - Expensive [24]<br>- Required filter weighing and cleaning [25]–[27]<br>- High power consumption [24]<br>- Bulky [12], [13] |
| Tapered Element Oscillating Microbalance (TEOM) (gravimetric) | Hollow, oscillating channel with a particle collection filter at its end [28]. Frequency counter records shift in oscillation frequency caused by a change in collected particle mass [25], [26]. | - Can provide real-time data [4]<br>- Widely used [12], [13] | - Expensive<br>- High power consumption<br>- Need filter cleaning or replacement [26]<br>- Humidity dependence can lead to inaccuracies, requires air heating [28]<br>- Bulky [12], [13] |
| Beta Attenuation Monitor (BAM) | Measure the attenuation of beta rays (i.e., electrons) by particles on a filter with a Beta radiation source and a Geiger-Mueller counter [29] | - Can provide real-time data<br>- Widely used [4], [7], [13], [29] | - Needs radiation source [29]<br>- Strongly influenced by humidity; can lead to inaccuracies, requires air heating [29].<br>- Expensive [24]<br>- High power consumption [12], [13]<br>- Bulky [12], [13] |
| Optical Particle Counter (OPC) | Direct a laser beam at particles and count their number from the resulting light scattering [5], [10], [30] | - Widely used<br>- Can be small and inexpensive [10], [21]<br>- Less power consumption than methods above [10], [21] | - Needs steady airstream<br>- Often limited accuracy [31], [32]<br>- Can be expensive [24]<br>- Calibration needed for each type of analyte [5], [30] |
| Micro Electro Mechanical System (MEMS) particle Sensors | Particles land on a resonating material and the resonant frequency shift caused by this is measured [22] | - Small and inexpensive [16]<br>- Easy to manufacture [33]<br>- Low power consumption [8], [14]–[21] | - Require improved accuracy [8], [14]–[21]<br>- Lower sensitivity [8], [14]–[21] |

sensing [23]. One of the main drawbacks of cantilever sensors is their low operating resonant frequency (typically up to the medium frequency range (MF, < 3 MHz)), which causes limited mass sensitivity [22]. Surface acoustic wave (SAW) resonators and bulk acoustic wave (BAW) sensors are other examples of MEMS sensors for particle sensing [8], [14]–[17], [19]–[21], [34]. In both types of sensors, a propagating or standing acoustic wave is excited in the piezoelectric material (zinc oxide or aluminium nitride, for example) by a voltage applied across metal electrodes.

Particle deposition increases the mass of the sensor and thus increases the wavelength of the acoustic wave. This leads to a decrease in the frequency of the same wave [8]. In 1959 the Sauerbrey Equation was developed to express this shift in the resonant frequency of a BAW quartz crystal microbalance (QCM), see Eq. 1. [35].

$$\Delta f_r = -\frac{\Delta m}{\rho A d} = -\frac{2 f_r^2 \Delta m}{A\sqrt{\mu\rho}} \qquad (1)$$

where the deposition of a mass $\Delta m$ on the surface of the crystal leads to a change in frequency, $\Delta f$. The film's density is expressed by $\rho$, $\mu$ is the elastic compliance of the film and its surface area is expressed by $A$ [36], [37]. For a BAW particle sensor, the independent variable in Eq. 1. is $\Delta m$. Thus, the frequency shift of the device is proportional to the deposited particle mass, which in turn means that the particle sensitivity of the resonator is also proportional to its resonant frequency [8], [16].

The small size and low power consumption of MEMS resonators makes them ideal candidates for a full system-in-package particle measurement system. They are comparatively inexpensive and easy to manufacture [16], [19]. Out of the two types, BAW devices have higher achievable resonant frequencies and smaller form factors than SAW resonators. This makes them in theory more sensitive to changes in mass deposition and thus, the desired option for particle sensing [16]. Film bulk acoustic resonators (FBARs) are one type of BAW device used for particle measurements. They consist of a thin piezoelectric film sandwiched between two metal electrodes. Typically, they use a cavity underneath the sensor and air on top of it to trap the acoustic energy in the piezoelectric layer [8].

To decrease the cost of a FBAR sensor system, combined complementary metal oxide semiconductor (CMOS) and MEMS technologies can be used. This enables full integration of the sensor with the required read-out circuitry. Complete system-on-chip devices could be made this way. CMOS

technology also enables large-scale manufacture, thus bringing the cost further down [8], [16], [21], [38]–[40]. Specht *et al*. have shown the particle mass detection capability of a film bulk acoustic wave resonator manufactured by SilTerra, Kulim, Malaysia in a combined 180 nm CMOS-BAW technology [8]. One challenge when combining these technologies is the creation of the cavity underneath the FBAR. Solidly mounted resonators (SMRs) are bulk acoustic wave devices where the air cavity underneath the sensor is replaced with an acoustic mirror called a Bragg reflector [33]. This eases manufacturing and increases CMOS compatibility [41]. It also increases device ruggedness and thus makes SMRs an interesting alternative to FBARs for real-world particle sensing [38]. Thomas *et al*. have demonstrated the use of such a device for particle sensing based on zinc oxide with discrete read-out circuitry [16]. To achieve high SMR quality factors the Bragg reflector stack needs to be designed carefully to suit the piezoelectric resonator. This means the thicknesses and materials of the layer stack need to fulfil very specific requirements related to the desired resonant frequency, for optimal reflection of the acoustic wave [38]. This could be a significant challenge in the mass manufacture of SMR devices because standard integrated circuit processes generally utilise process-specific layer thicknesses [33], [38]. There is thus a trade-off between ease of manufacturing through the standard process and resonator quality. In 2019 Villa López *et al.* demonstrated the functionality of a standalone SMR sensor based on an oxide/tungsten CMOS Bragg reflector stack fabricated using a standard CMOS process. An aluminium nitride resonator was deposited in post-processing [38].

The work presented here demonstrates the design and experimental evaluation of an aluminium nitride SMR particle sensor designed at the University of Warwick, UK and manufactured by SilTerra in a combined 180 nm CMOS-BAW process. The work also demonstrates the sensor's increased sensitivity through temperature-frequency modulation. The novel device achieves temperature control and thermal modulation through an integrated microheater realised underneath the integrated Bragg reflector in the CMOS metallisation layer [33]. Specht *et al*. demonstrated the effect of varying heater current on the output frequency of the read-out oscillator circuit in [33].

The idea exploited in this paper is that particles settling on the sensor will increase the thermal time constant of the device, dependent on mass and surface area. Simulations of this effect are firstly conducted and are presented in this work. In these, a current is applied to the microheater to increase/decrease the temperature of the resonator. This should alter the transient change in resonant frequency caused by the temperature gradient. This work thus aims to show the use of temperature modulation for significantly improved particle sensitivity and a lower detection limit of a novel SMR particle sensor.

Following simulations, the effects of thermal modulation on the performance of the particle sensing system are experimentally investigated and results presented in this paper. In these tests a set of two SMR sensors is used in a differential configuration where one SMR is used as a sensing device and another as a reference. A pulsed current is applied only to the microheater of the sensing SMR. In the first set of the experiments, the SMR particle sensor relies on the random settling of particles on the sensor surface. In the second part, the sensor is combined with a fan-driven channel and thermophoretic particle sampling system. In addition to the improved performance through the temperature modulation, this type of setup increases particle sampling efficiency and repeatability. This further demonstrates that the novel SMR particulate matter sensing system is a good candidate for applications in air quality monitoring.

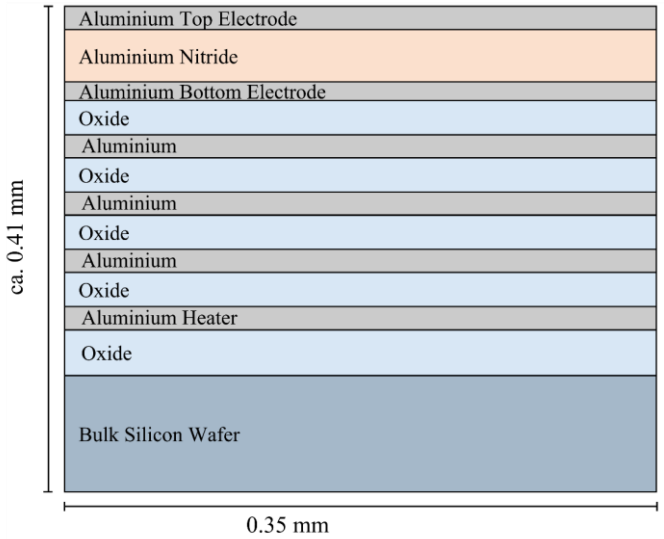


**Fig. 1.** *Cross-Section of CMOS SMR layer stack.*

## II. Design and Simulation of CMOS SMR

### *A. Design of CMOS SMR*

The CMOS SMR designed in this work comprises a resonator and a Bragg reflector fabricated using standard layer materials and thicknesses of SilTerra's 180 nm CMOS-MEMS/BAW technology. Using a standard CMOS process results in lower cost of manufacturing and ease of integration at the expense of a less optimised Brag reflector stack, which in turn leads to a lower resonator Q factor [33]. Fig. 1 shows a cross-section of the device layers.

The resonator consists of a 1.3 µm aluminium nitride film sandwiched between a 400 nm thick bottom and a 350 nm thick top electrode made of aluminium. The Bragg reflector stack is formed by three 850 nm thick oxide layers interspaced with three, 530 nm thick, aluminium metal layers of the 180 nm CMOS process. The bottom metal 1 aluminium layer is used for the integrated heater. It has a resistance of about 52 Ω at room temperature. The SMR device's substrate is a 400 µm thick silicon wafer. Fig. 2 shows the cross section of the manufactured layer stack recorded with a scanning microscope. It was measured that the fabricated CMOS layers are within about five percent, and the BAW layers are within about one percent of the process specified thicknesses. A top-view image of the manufactured SMR is shown in Fig. 3.

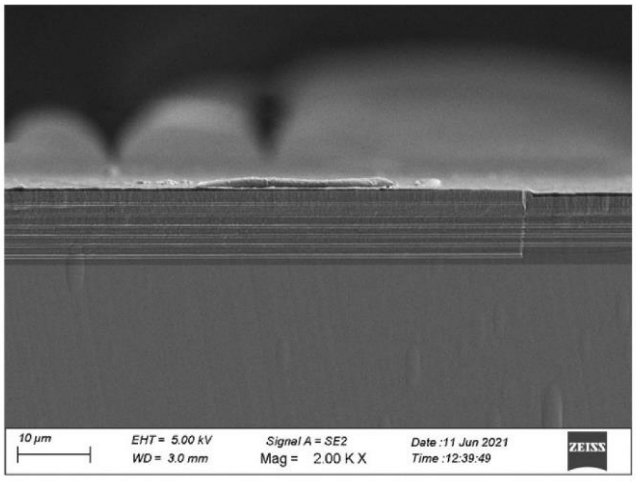


**Fig. 2.** *Cross-section of CMOS SMR SEM image of the manufactured device.*

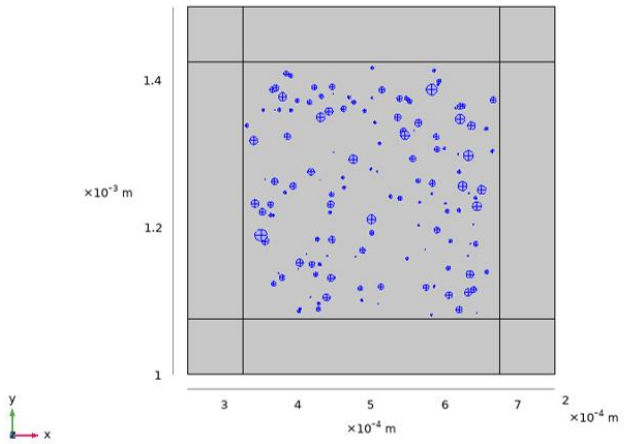


**Fig. 4.** *COMSOL model of active area with particles.*

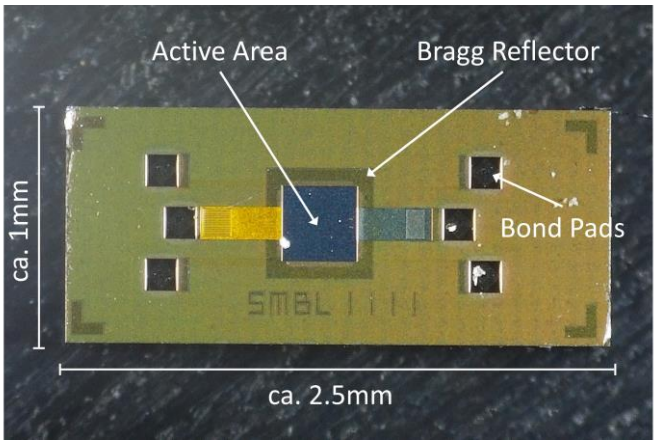


**Fig. 3.** *Top-view of manufactured CMOS SMR.*

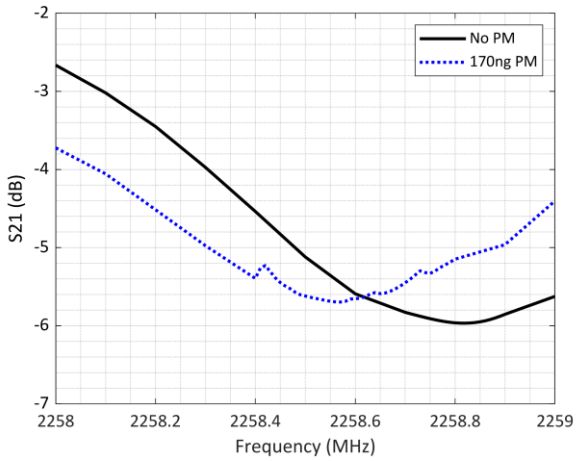


**Fig. 5.** *FEM S21-parameter of the CMOS SMR active area with 170 ng of particles.*

*B. COMSOL modelling results and comparison with the fabricated device*

Prior to manufacture, a finite element model of the device was simulated to confirm the functionality of the sensor. The simulations were conducted using the MEMS and the Heat Transfer modules of COMSOL Multiphysics® v5.5. The integrated material libraries were used to obtain the material parameters. The device was simulated with and without particle deposition and with and without temperature control [33].

To confirm whether the sensor is sensitive to particles in principle, only the active area of the resonator was simulated. This was to reduce the hardware requirement for the computations. Three-dimensional frequency domain studies were used to calculate the resonant behaviour of the SMR. In these the SMR electrodes were excited with a power of about 0.1 W. A terminated terminal interface was then used to obtain the S21 parameter directly from the model. Fig. 4 shows the top-view of the active area of the SMR covered by particles as it was modelled in COMSOL.

COMSOL's integrated pseudorandom number generator was used to set the particle position and diameter on the sensor surface with the same size distribution as the particles used for the experimental tests. The test dust used is the aerosolised type ISO 12103-1 A1 "Ultrafine" dust. Its main constituent is quartz. The maximum particle size is 20 µm and the average particle size is 6 µm. The density is 2500 kg/m$^3$. In the simulations, the particles were assumed to be spherical and perfectly bonded to the resonator surface with stable ambient conditions and no airflow. The active area of the SMR resonates at about 2258.8 MHz, with an S21 of approximately -6 dB. The deposition of 170 ng of quartz particles up to 20 µm diameter (see Fig. 4) shifted the resonant frequency by about 200 kHz and changed S21 by about 0.25 dB. This simulation result is shown in Fig. 5.

The temperature dependence of the SMR resonant frequency was investigated, too. For this the whole substrate of the sensor was simulated. The thermal variation of the relevant properties of AlN [42] and the temperature dependence of the CMOS aluminium conductivity were included in the model. The frequency domain study was then repeated without particles to

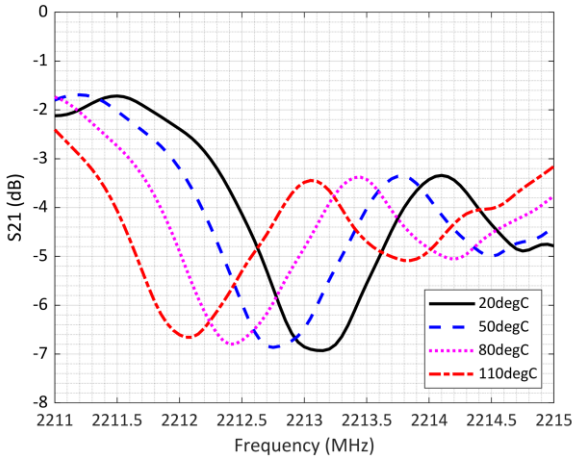


**Fig. 6.** *FEM S21-parameter of the CMOS SMR sensor at different temperatures.*

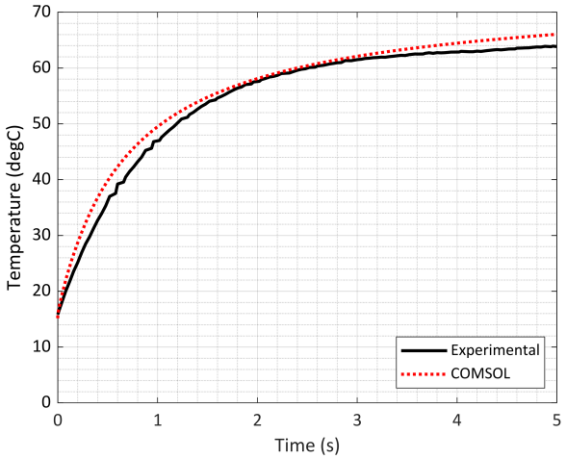


**Fig. 8.** *Device temperature vs. time on printed circuit board (PCB).*

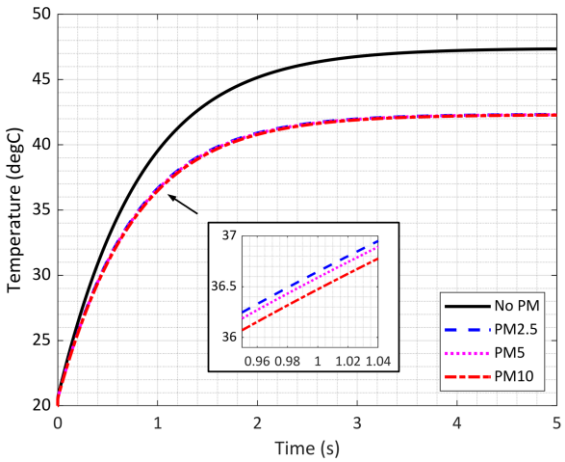


**Fig. 7.** *Device temperature vs. time (COMSOL simulations).*

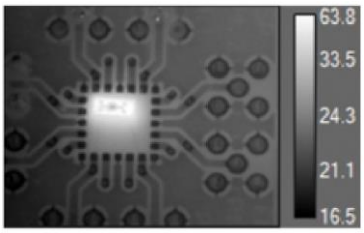


**Fig. 9.** *FLIR SC7000 image of the heated device.*

obtain the resonator behaviour at different temperatures of 20, 50, 80 and 110 °C. The S21-parameter calculated in this study is plotted against frequency in Fig. 6.

At 20 °C a S21 value of -7 dB at a frequency of about 2213 MHz is calculated. A Q-factor of approximately 1200 is estimated when dividing the resonance by the 3 dB bandwidth. In the simulations, the resonant frequency decreased by about 10 kHz per degree change in temperature.

The manufactured SMR's resonant frequency was found to be about 2000 MHz, with an S21 of -6 dB and a change in the resonant frequency of about 70 kHz per degree change in temperature, as is shown in [33]. The Q factor was measured to be about 200 [33].

The integrated microheater is designed to be capable of heating the sensor to temperatures between room temperature (20 ºC) and about 300 ºC [33]. This was confirmed in a stationary study simulating electromagnetic heating in COMSOL®. Approximately linear thermal variations in heater resistance between 50 and 65 Ω over a SMR temperature range of 15 to 300 °C were calculated.

This work aims to increase the sensitivity of the SMR particle sensor by applying thermal modulation. The steady state temperature and thermal time constant of the sensor was first calculated. This was done with particle mass loading and with a current of 33 mA applied to the heater. For these thermal simulations the setup assumed external natural convection at about 20 °C. The model further assumed the device was a perfect black body to model radiative heat loss. The steady-state temperature at different heater currents was first calculated in a stationary study to determine the thermal time constant temperature. Once this was known, a transient analysis was executed only to the point in time where the temperature passes two thirds of that value. This reduced the computational effort. Domain probes were used to record the average temperature of the active area of the aluminium nitride layer at intervals no larger than 0.05 s. In the thermal study the particles were modelled by adding a solid layer of quartz of different thicknesses (corresponding to the sizes of particulate matter of interest) onto the entire top surface of the sensor. The result is plotted in Fig. 7. In this simulation, placing the layer of quartz onto the sensor surface results in temperature drops of the device by approximately 5 °C. The thermal time constant for the "No PM" plot is about 0.95 s. It increases to about 1.00 s for PM2.5. This corresponds to a change of about five percent. The value increases slightly to 1.01 s for PM5 and 1.02 s for PM10.

Fig. 8 shows the transient temperature change of the SMR surface when a current of 60 mA is applied to the heater while

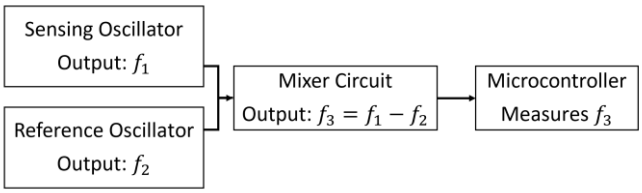


**Fig. 10.** *Diagram of differential sensor configuration.*

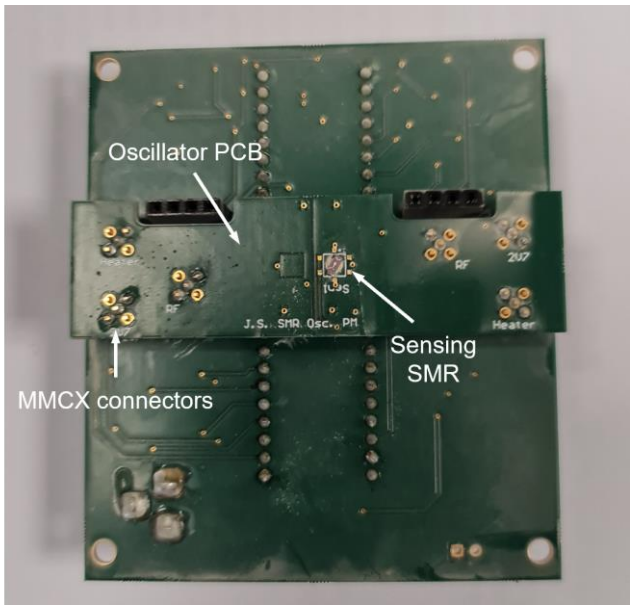


**Fig. 11.** *Setup of particle sensor (top-view).*

the device is mounted onto a printed circuit board (PCB; in red). From this result, a thermal time constant of approximately 1.97 s was calculated. The experimental thermal transient at the same current was recorded with a SC7000 infrared camera by Teledyne Forward-looking Infrared® (FLIR) and is shown in Fig. 8 in black. Fig. 9 shows a SC7000 infrared image of the heated SMR. The thermal time constant of the fabricated device can be read to be approximately 1.85 s: about 10 percent under the theoretical value.

Increasing the SMR microheater current, the oscillating frequency of the oscillator decreased by about 300 kHz. This is comparable to data on the same sensor published by Specht *et al*. [33].

## III. Experimental Setup

### *A. Drive Circuit Details*

A disadvantage of MEMS resonators is that direct measurement of the resonant frequency of a piezoelectric device requires expensive and bulky equipment [16]. To resolve this, MEMS resonators are often used as the frequency setting element in the feedback loop of a sinusoidal voltage oscillator circuit. This exploits the shift in the frequency of the oscillator output voltage observed when the sensors' resonant frequency changes [8], [16], [20]. It can be measured easily using timer circuits on standard microcontrollers. However, to achieve high

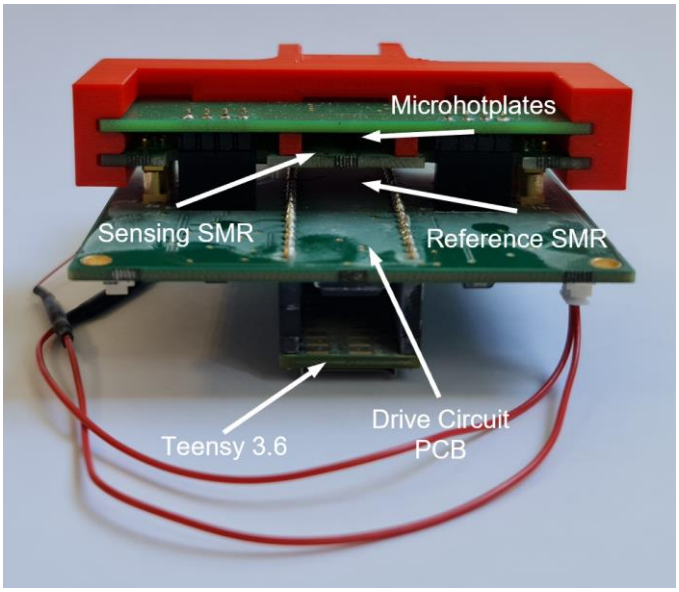


**Fig. 12.** *Setup of particle sensor with microchannel (back-view).*

particle sensitivity with MEMS resonators, resonant frequencies in the very high and the ultra-high frequency (VHF and UHF) range need to be used. This makes oscillator frequency measurement more challenging. Sophisticated equipment is also needed to measure UHF range voltage signals [16]. Several works have demonstrated the use of a frequency mixer with a reference oscillator as a possible solution that has been utilised in this work. A schematic of this differential measurement principle is shown in Fig. 10.

The mixer outputs the difference between the reference and the sensing oscillator's frequency. This results in a read-out signal with a lower frequency that can then be measured with standard equipment. In this, only the frequency of the sensing oscillator, is affected by the particles. Thus, the absolute change in frequency remains unaffected in the differential configuration [8]. Several works have done this by using a second oscillator circuit as a reference isolated from particles [8], [16], [20], [34]. The use of a reference device also helps to minimise common mode effects [8], [11]. This, for example, minimises thermal noise and humidity variation effects that can cause drift in both devices. This way the effect of particles settling on the sensing oscillator can be reliably measured [8], [16], [20]. The oscillator configuration used here is the Pierce oscillator used by Specht *et al.* implemented on a PCB in the differential configuration [33].

For the experimental tests the sensing SMR is wire bonded to the upside of this PCB. The board also carries the two Pierce oscillator circuits: one for the sensing SMR and one for the reference SMR. The reference SMR is mounted outside the channel on the lower side of the PCB to stop particles from landing on its surface. Fig. 11 shows a photograph of the SMR bonded on the oscillator PCB with the associated circuitry.

The sensors are held in place using thermally conductive silicone paste. Micro-miniature coaxial (MMCX) connectors are used to connect the Pierce oscillator board with the

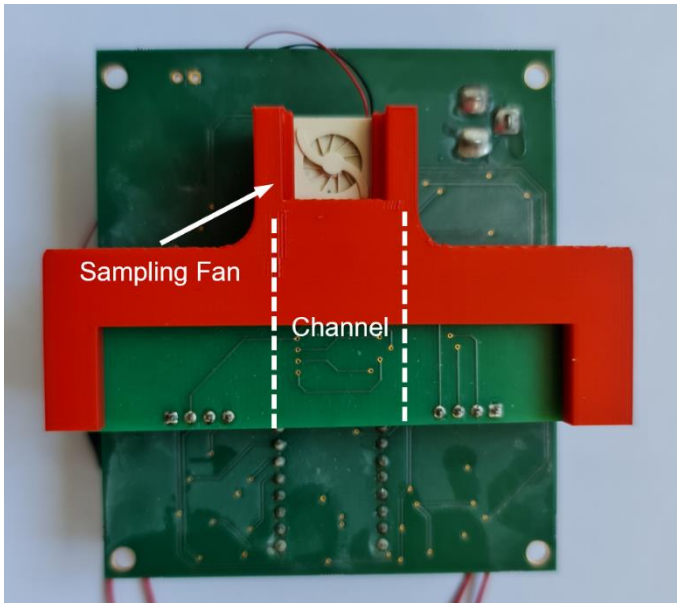


**Fig. 13.** *Setup of particle sensor with microchannel (top-view).*

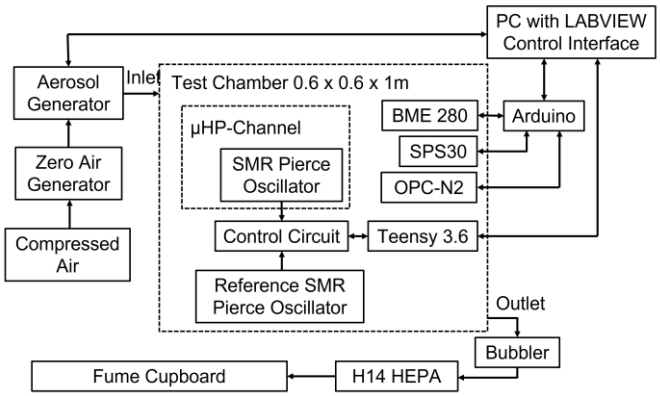


**Fig. 14.** *Functional block diagram of particle test rig.*

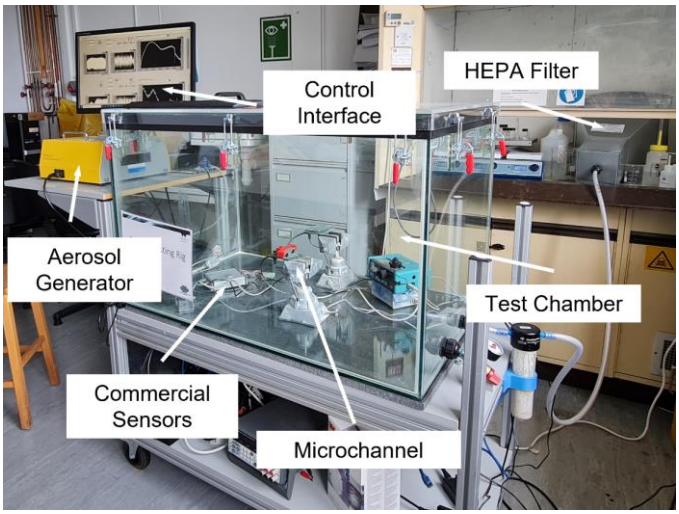


**Fig. 15.** *Photograph of particle test rig.*

associated SMRs to the 3.3 V power supply, the frequency read-out, and the heater drive circuitry. 3.3 V is a regulated supply available on the Teensy 3.6 microcontroller. A Teensy 3.6 microcontroller is plugged into the lower side of the drive circuit for frequency counting and to provide the sensor power supply. It is also used for data transmission to and from the LABVIEW interface on a computer used for external control of the system.

The drive circuitry comprises an Analog Devices AD8302 gain and phase detector to detect the difference in signal strength between the two oscillators. A Mini-Circuits RMS-30+ mixer circuit is used to output the difference in resonant frequency between the oscillators. A comparator is used to increase the signal from the mixer circuit to the logic level of the timer circuit of the Teensy 3.6 microcontroller. The comparator output signal frequency is measured three times per second and recorded through the LABVIEW interface.

In the first set of the experiments, the SMR particle sensor relies on the random settling of particles on the sensor surface. In the second part, the sensor is combined with a fan-driven channel and thermophoretic particle sampling system.

Fig. 12 and Fig. 13 show the sensor device with the 3D-printed microchannel used for the second set of experiments. The channel slides onto the PCBs onto which the sensors and the micro hotplates needed for the thermophoretic sampling are mounted. They form the top and bottom walls of the channel. The microhotplates are integrated on a single substrate as an array of eight [8]. They are glued and wire bonded to the underside of the top PCB

The microhotplate PCB is connected to the PCB with the drive circuitry by using standard 2.54 mm spaced pin headers. The headers and connectors also ensure a tight fit of the boards on top of each other. The drive circuitry also contains a set of constant current sources to power the microhotplate array and the integrated SMR heaters.

The heaters' switching frequencies and temperatures are controlled by using the Teensy to switch between current sources via a set of BSN20 metal oxide semiconductor field effect transistors (MOSFETs). The setup is powered from the mains by means of a 220 V to 12 V AC to DC rectifier. The power draw of the whole system is about 550 mW when the SMRs operate at about 50 °C and the microhotplates at about 400 °C. The SMR microheater's current was varied between zero and 33 mA with a 50% duty cycle and a period of 30 s.

### *B. Schematic of test rig*

The experimental setup and procedure used to acquire the data for this paper follows that of Specht *et al.* in [8]. A schematic representation of the test rig is shown in Fig. 14. A TOPAS SAG410/L aerosol generator has a compressed zero air supply to feed aerosolised ultrafine Arizona dust into a sealed test chamber at 1 bar air pressure [8]. The room in which the chamber is situated is temperature controlled through air conditioning. A Bosch BME280 sensor was used to monitor the humidity, temperature, and pressure inside the test chamber. The microchannel is held at the centre of the test chamber with a vice. A LABVIEW desktop interface allows centralised control of the test rig, and it allows the monitoring and

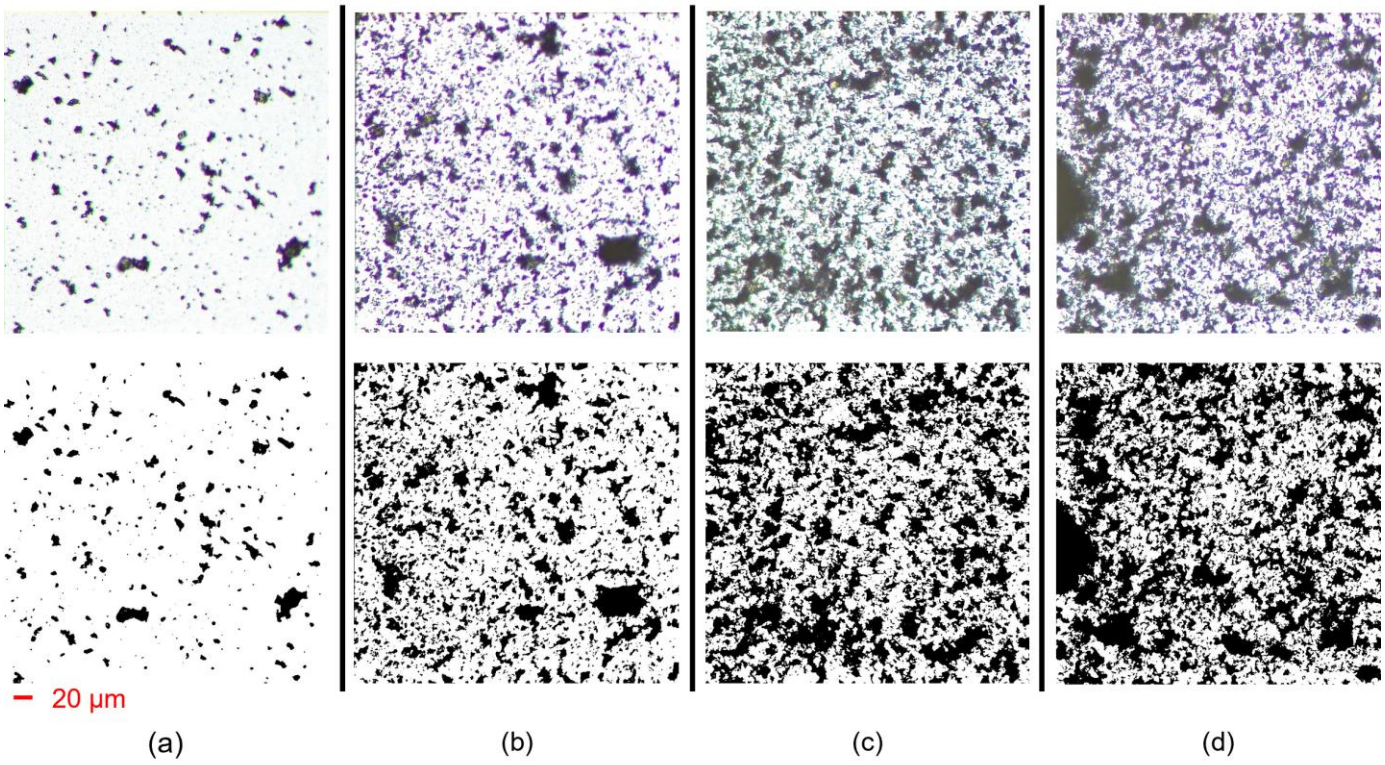


**Fig. 16.** *Original (top) and binarised (bottom) image (Leica ICC50 W) of top electrode after tests with increasing particle feed rate from (a) 9.5 (b) 19 (c) 43 (d) 66 µg/m³s.*

recording the data from all devices in real time [8]. A photograph of the complete test setup is shown in Fig. 15.

### *C. Experimental Methodology*

Compressed zero air is set to flow into the chamber for the entire duration of the test to ensure consistent temperature, pressure, and humidity levels. The SAG410/L aerosolises particles into the airstream depending on the speed setting of an internal feeding belt, which was varied between 2, 5, 10, 15 % of full speed, corresponding to 0.1, 0.25, 0.5 and 0.75 V.

Three tests were run for each particle feed setting. The particles were cleaned from the chamber between the tests. After each test, the SMR surface was photographed using a Leica DM750M microscope with 20× zoom and a 5 MP Leica ICC50 W camera. The SMR and the microchannel were then cleaned with compressed air [8]. The sensor was first tested without and with thermal modulation and without the microchannel sampling system. It was then tested with both thermal modulation and the microchannel. Once the chamber temperature, pressure and humidity reached a stable point, the particle injector of the SAG410/L was enabled for five minutes and then disabled. This led to maximum particle concentrations of approximately 500, 1000, 2000 and 3000 µg/m$^3$ as measured by a commercial particle sensor (Alphasense Ltd, OPC-N2) [8]. To calculate the mass of the particles, the images of the SMR surface were cropped down to the top electrode and then binarised using MATLAB. From this, the fraction and hence the area of the electrode surface covered with particles was calculated. Assuming an average particle diameter of about 6 µm, the volume of the particles was multiplied by the density of the Arizona dust (2500 kg/m$^3$) to give the particle mass.

## IV. Results from Experimental Particle Testing

To determine the mass sensitivity of the SMR and the achievable improvement in sensitivity by temperature modulation, the device was first tested without any sampling system; it relied on random particle settling only. Fig. 16 shows images of the SMR device's top electrode taken after test runs at each of the four particle concentrations investigated, and the binarised version of these images used to calculate the particle mass.

The Alphasense OPC-N2 particle sensor measured maximum PM10 concentrations of approximately 500, 1000, 2000 and 3000 µg/m$^3$. It can be seen from Fig. 16 that the number of particles settled onto the top electrode increases significantly with the increased particle concentration. The lighting and focusing conditions of the images vary slightly, because of slight variations in the manual positioning of the sensor under the camera lens after each test. This however did not affect the binary version of the images, see Fig. 16.

The normalised frequency of the mixer circuit's output signal sampled over time is shown in Fig. 17 and Fig. 18. Fig. 17 shows typical data from one test run for each particle concentration tested without thermal modulation. Fig. 18 shows the same for the temperature modulated signal. Both were filtered with a 255-point moving average filter to remove noise effectively. This made the shift easier to see in the modulated

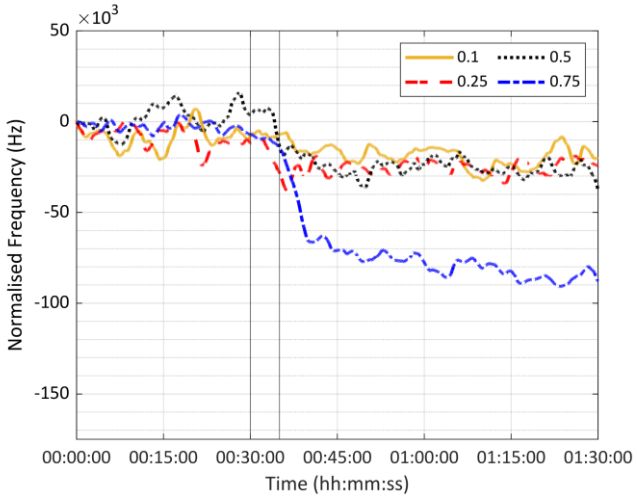


**Fig. 17.** *Normalised, filtered mixer output signal without temperature modulation with vertical lines indicating duration time of particle injection into the chamber.*

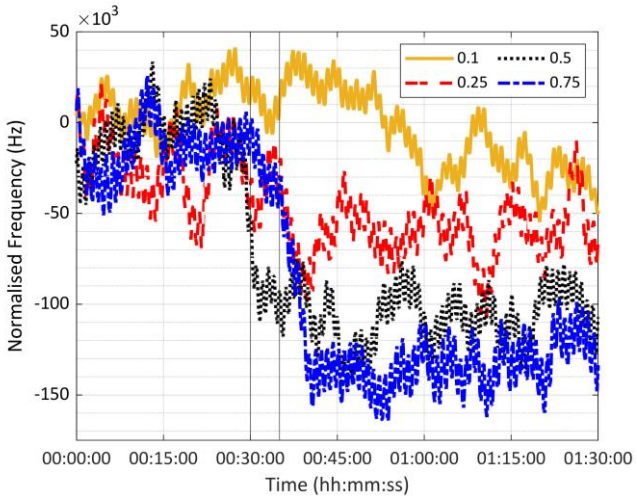


**Fig. 18.** *Normalised, filtered mixer output signal with temperature modulation with vertical lines indicating duration time of particle injection into the chamber.*

frequency signal. The vertical, black lines indicate the time during which particles are injected into the chamber. Apart from some random noise variations there is no visible output signal drift during the tests.

It was observed that it takes about 30 minutes for the particle concentration to drop back close to its initial level. This settling of aerosolised particles after the feed is turned off leads to an additional, slow drop in frequency seen in Fig. 17 and 18. The variation of the relative humidity inside the test chamber is plotted during a high particle concentration test in Fig. 19. It does not correlate to the trend in resonant frequency. Similarly, no visible correlation was observed between the temperature and frequency measurements as shown in Fig. 20.

From Fig. 17, without modulation, the sensor exhibits the frequency shift of approximately 10 kHz, 15 kHz, 25 kHz, and 60 kHz as the concentration of particulate matter is increased

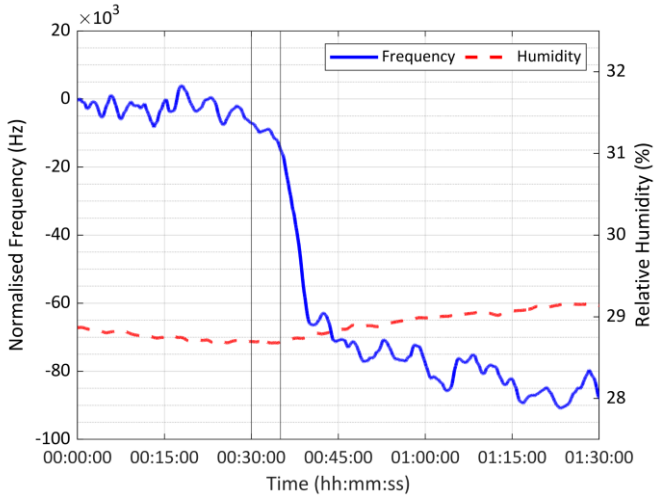


**Fig. 19.** *Variation of test chamber humidity during experiment.*

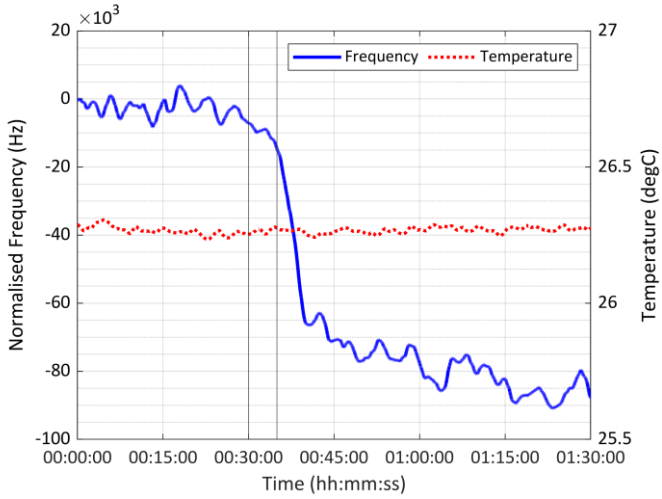


**Fig. 20.** *Variation of test chamber temperature during experiment.*

from 500 µg/m$^3$ to 3000 µg/m$^3$. From Fig. 18 the shift increases considerably to about 15 kHz, 50 kHz, 130 kHz, and 140 kHz, respectively, when temperature modulation is applied (values rounded to the nearest 5 kHz).

The frequency shifts from repeated test runs are plotted against the particle mass settled on the sensor surface in Fig. 21. The particle masses are those that were estimated from the binary images. The positive gradient of the lines of best fit indicates that a larger particle mass on the sensor surface leads to a larger shift in the resonant frequency of the sensor. Hence Fig. 21 shows that the shift in resonant frequency is proportional to the settled particle mass. This confirms the functionality of the SMR device as a particle sensor.

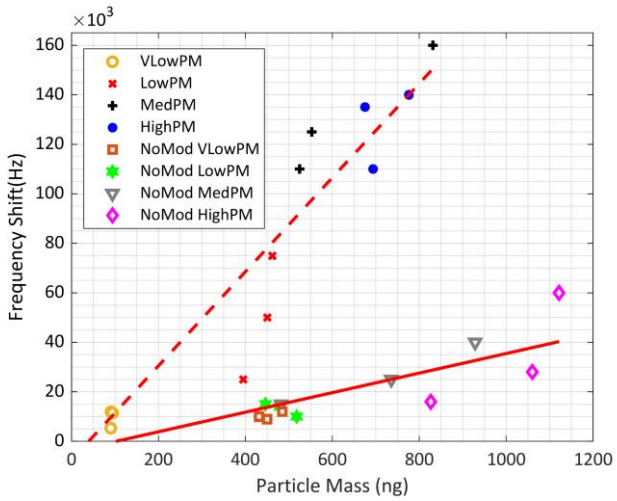


**Fig. 21.** *Resonant frequency shift vs. particle mass on top electrode.*

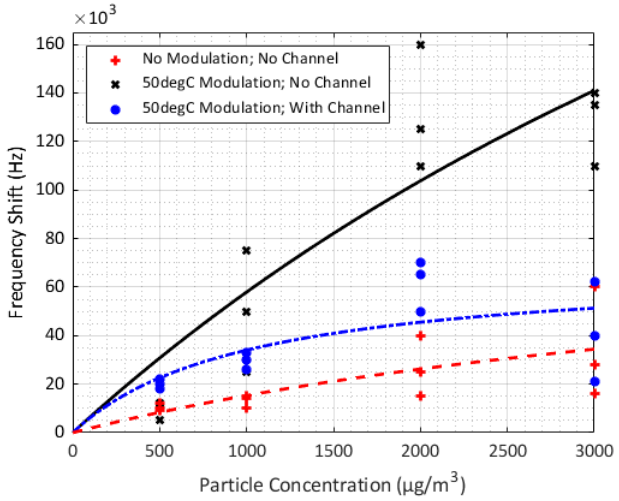


**Fig. 22.** *Resonant frequency shift vs. particle concentration in chamber.*

Without modulation the gradient is 40 Hz/ng, see Eq. 2. When temperature modulation is applied to the device, this increases to 190 Hz/ng, see Eq. 3, where $m$ is the particle mass on the top electrode and $\Delta f$ is the resulting shift in resonant frequency.

$$\Delta f_{non-modulated} = 40m - 4000 \quad (2)$$

$$\Delta f_{modulated} = 190m - 7500 \quad (3)$$

The detection limit can be read from Fig. 21 to be 100 ng and 50 ng of particles, respectively.

A reduction in Pierce oscillator signal strength from the lowest to the highest particle concentration setting of about 0 dB, 0.02 dB, 0.07 dB and 0.12 dB, respectively, was detected when modulating the resonator temperature. No observable change in signal strength was measured when the SMR microheater was not used.

As mentioned above, the set of tests was repeated with a fan-driven channel and thermophoretic particle sampling system [8] to avoid relying only on random particle settling. Fig. 22 shows the frequency shifts plotted against the particle concentrations. It includes data (in blue) from experimental runs with the thermophoretic particle deposition mechanism. The lines of best fit are based empirically on a Langmuir isotherm [8]. They are given by Eq. 4, Eq. 5 and Eq. 6 below.

$$\Delta f_{Snon-modulated} = \frac{9.1 \times 10^4 \times 2.0 \times 10^{-4} \times C}{1 + 2.0 \times 10^{-4} \times C} \quad (4)$$

$$\Delta f_{Smodulated} = \frac{5.0 \times 10^5 \times 1.3 \times 10^{-4} \times C}{1 + 1.3 \times 10^{-4} \times C} \quad (5)$$

$$\Delta f_{Schannel} = \frac{6.7 \times 10^4 \times 9.8 \times 10^{-4} \times C}{1 + 9.8 \times 10^{-4} \times C} \quad (6)$$

Here $C$ is the particle concentration and $\Delta f_S$ is the corresponding frequency shift.

Fig. 22 shows that frequency shifts of the SMR sensors during the tests with the sampling channel and thermal modulation are improved compared to the tests without the channel and modulation (fitted curve up to 50 kHz compared to 35 kHz). It can be observed that the efficiency of the sampling channel is reduced at higher particle concentrations. This is indicated by the increasing spread in frequency shifts (~40 kHz at 3000 µg/m$^3$ compared to 20 kHz at 2000 µg/m$^3$) and by their reduction in magnitude (20 to 60 kHz at 3000 µg/m$^3$ compared to 50 to 70 kHz at 2000 µg/m$^3$). Measured frequency shifts at each concentration are not as high as when the resonator was thermally modulated without using the sampling channel (up to 70 kHz compared to up to 160 kHz). However, the frequency shifts measured with the sampling channel show increased repeatability at lower particle feed settings. With temperature modulation the spread of measured frequency shifts is reduced from 7 kHz without the channel to 4 kHz with the channel at 500 µg/m$^3$, from ca. 50 kHz to 7 kHz at 1000 µg/m$^3$ and from 50 kHz to 20 kHz at 2000 µg/m$^3$. On average this is a reduction in the spread of shift measurements at each concentration setting from 36 kHz to 10 kHz.

## V. Discussion of Results

The main aim of this work was to demonstrate the potential of employing SMR sensors in air quality monitoring by increasing their sensitivity to particulate matter by means of thermal modulation. Both simulation and experimental results show promising results.

Prior to fabrication the extensive set of simulations was performed. The devices were simulated and designed to operate at 2.2 GHz resonant frequency with fabricated devices operating at 2 GHz. Differences in absolute SMR resonant frequency can be mainly explained by uncertainties in the material properties. A difference in CMOS layer thickness of up to five percent could also have contributed to the discrepancy between theoretical and practical values.

The thermal time constant of the sensor was calculated with and without particle mass loading. A change of about 5 % was observed when the device was loaded with PM2.5 particles.

This increased further when loaded with PM5 and PM10. When a current of 60 mA was applied to the heater the thermal time constant was calculated to be approximately 1.97 s. The SMR temperature was approximately 70 °C. The experimentally determined thermal time constant was approximately 1.85 s: about 10 percent different from the theoretical value. The perfectly stable environmental factors assumed in the simulations is a potential cause of this difference between the expected and the practical resonator temperature coefficient of frequency and the quality factor. The assumption of only natural convection being present is another possible cause. There is a constant turbulent flow of zero air through the test chamber over both the sensing and the reference device. This would cause some degree of heat loss through forced convection. Differences in sensor positioning also exposes the resonators to slightly different airflows which explains the slight offset of resonant frequency baseline seen in Fig. 18.

Increasing the thermal mass of the thermally modulated resonator through particle deposition has also led to a loss in oscillator signal strength up to 0.12 dB. This contrasts with no observable signal damping without temperature modulation.

These factors result in a change of oscillation frequency each time the heater changes its power stage, and hence greater frequency sensitivity per unit mass deposited, (see Fig. 21). Plotting a line of best fit onto the data shows the shift in SMR resonant frequency is proportional to the particle mass deposited on the resonator surface with a sensitivity of approximately 40 Hz/ng. This was expected, as a larger mass corresponds to a lower resonant frequency according to the Sauerbrey equation [35]. Adding temperature modulation improved SMR sensitivity to particulate matter by a factor of approximately five to 190 Hz/ng. It also halved the detection limit of the sensor from 100 ng down to 50 ng. It can be seen in Fig. 21 that the effect of thermal modulation is stronger when a larger particle mass is deposited. These results were expected because a larger mass of potentially larger particles affects both the frequency and the thermal mass stronger than a smaller mass of particles. This translates into a steeper gradient of frequency over deposited particle mass.

When compared to the simulations the observed frequency shift caused by a unit particle mass on the top electrode is significantly smaller in the experimental tests (approximately 200 kHz compared to 10 kHz). This can be explained by assumptions made in the model, such as perfect coupling between the surfaces of the particles and the top electrode of the device. Additionally, the simulations only calculated the resonant frequency of the sensor based on its active area. This means that the particles cause a larger relative change in the mass of the studied device, which could also explain the larger change in resonant frequency. Another possible reason is inaccuracy in the calculation of the particle mass from the experimental tests caused by the assumption of constant particle diameter in the direction of the z-axis. This might cause an overestimation of the deposited particle mass since much of the area shown in Fig. 16 is covered by particles with a diameter smaller than 6 µm in all directions.

Experiments were conducted with and without sampling system. Better repeatability of the resonant frequency shift was achieved with the microchannel sampling for a given setting of particle concentration. Thus, the device's reliability for aerosolised particle sensing is higher. Particle deposition is controlled by thermophoresis in this setup, as opposed to the random settling without the microchannel. This can be seen to cause high variability in analyte mass on the sensor surface (up to 250 ng), according to Fig. 21. The channel does seem to reduce the sensitivity of the resonator for direct particle mass sensing, however. This is most likely because of greater resonator cooling caused by the sampling fan. It would reduce the difference in temperature between the bare resonator and the resonator after particle deposition. The microchannel also reduces the upper detection limit of particle mass. This can be observed from the drop in frequency shift at the high concentration end of Fig. 22. A mixture of factors could be the reason for this, for example, a reduction in the effectiveness of the thermophoretic effect caused by greater cooling of the channel air at large particle concentrations. An effect of this might also be that more particles remain aerosolised while in the channel, and thus leave the channel before they have settled on the resonator surface. However, the improvements of device operation observed at lower particle concentrations are more significant since these are closer to the concentration observed in an urban environment [8].

A 12 V DC power supply powered the device in this paper, but the measured power consumption of approximately 0.55 W means that it would be possible to power the whole setup with the 0.85 W power supply from a Teensy 3.6 microcontroller at 3.3 V. Doing so could enable the device to function as a personal particle monitor and enable easy powering of the setup through standard batteries. This is another improvement compared to current commercial low-cost particle sensing devices, such as the Alphasense OPC-N3. The latter has a typical power consumption of about 0.9 W.

## VI. Conclusion

A novel, low-cost, CMOS-compatible device with an integrated microheater was designed and manufactured in a standard 180 nm CMOS-BAW process. It was combined with a read-out circuitry into a complete sensor system with low power consumption. A substantial improvement of a solidly mounted resonator particle sensor through temperature modulation was observed. The effect of temperature modulation was first investigated through finite element modelling and then confirmed experimentally. Particle deposition was found to increase the thermal time constant of the solidly mounted resonator with pulsed heating by approximately 5 %. This led to an increased shift in device resonant frequency. This effectively amplified the mass sensitivity of the sensor from 40 Hz/ng to 190 Hz/ng. This effect was observed to be stronger at higher particle concentrations. It was also demonstrated that the thermally-modulated solidly mounted resonator particle sensor could be used as a more reliable device for aerosolised particulate matter monitoring when combined with a sampling system. This comprised a fan for air sampling and a thermophoretic particle deposition setup.

The average spread of data for the tested settings was shown to reduce from 36 kHz to 10 kHz. It was confirmed that thermophoretic particle deposition works more effectively for low particle concentrations. Future work will include modulating the heater with a higher power to test the effect of larger temperature swings on the resonant frequency shift. This might result in higher amplification. The further tests will also include testing the effect of temperature modulation on particles of different materials to investigate the potential to discriminate particles both in terms of size and type. Optimising the solidly mounted resonator design, by fine-tuning the layer thicknesses to the optimum, or using a higher acoustic impedance material than aluminium to improve the Bragg reflector, could further improve the performance of the devices. However, this would be at the expense of a higher fabrication cost. It would make CMOS compatibility of the setup more difficult to achieve. Optimising the circuitry further to reduce power consumption and using Silterra's standard CMOS-BAW process to integrate the circuitry on the same substrate as the sensor can result in a complete system-on-chip particle sensor. Future work could also include testing a larger range of particles, especially lower particle concentrations, and some in-situ testing of the device outside of a laboratory environment.

## ACKNOWLEDGMENT

The The authors gratefully acknowledge SilTerra's MEMS and SENSORS technology Business Unit in Kulim, Malaysia, for the manufacturing of the CMOS compatible SMR devices designed in this work.

The authors would also like to thank Frank Courtney at the University of Warwick for his assistance in manufacturing the 3D-printed channel.

## REFERENCES AND FOOTNOTES

[1] X. Wu, R. C. Nethery, M. B. Sabath, D. Braun, and F. Dominici, "Air pollution and COVID-19 mortality in the United States: Strengths and limitations of an ecological regression analysis," *Science Advances*, vol. 6, no. 45, p. eabd4049, Nov. 2020, doi: 10.1126/SCIADV.ABD4049.

[2] A. Solimini *et al.*, "A global association between Covid-19 cases and airborne particulate matter at regional level," *Scientific Reports*, vol. 11, no. 6256, Mar. 2021, doi: 10.1038/s41598-021-85751-z.

[3] N. S. M. Nor *et al.*, "Particulate matter (PM 2.5) as a potential SARS-CoV-2 carrier," *Scientific Reports*, vol. 11, no. 1, p. 2508, Jan. 2021, doi: 10.1038/s41598-021-81935-9.

[4] U.S. Environmental Protection Agency, "Policy Assessment for the Review of the National Ambient Air Quality Standards for Particulate Matter.," Research Triangle Park, Jan. 2020. Accessed: Jul. 13, 2021. [Online]. Available: https://www.epa.gov/naaqs/particulate-matter-pm-standards-policy-assessments-current-review-0

[5] L. Lombardo, M. Parvis, E. Angelini, and S. Grassini, "An Optical Sampling System for Distributed Atmospheric Particulate Matter," *IEEE Transactions on Instrumentation and Measurement*, vol. 68, no. 7, pp. 2396–2403, Jul. 2019, doi: 10.1109/TIM.2019.2890885.

[6] D. Giannadaki, J. Lelieveld, and A. Pozzer, "Implementing the US air quality standard for PM 2.5 worldwide can prevent millions of premature deaths per year," *Environmental Health*, vol. 15, no. 1, p. 88, Aug. 2016, doi: 10.1186/S12940-016-0170-8.

[7] B. I. Magi, C. Cupini, J. Francis, M. Green, and C. Hauser, "Evaluation of PM2.5 measured in an urban setting using a low-cost optical particle counter and a Federal Equivalent Method Beta Attenuation Monitor," *Aerosol Science and Technology*, vol. 54, no. 2, pp. 147–159, Feb. 2020, doi: 10.1080/02786826.2019.1619915.

[8] J. P. Specht *et al.*, "AlN FBAR Particle Sensor with a Thermophoretic Sampling Mechanism," *IEEE Sensors Journal*, vol. 21, no. 17, pp. 19427–19435, 2021, doi: 10.1109/JSEN.2021.3086528.

[9] P. Castello, C. Muscas, P. A. Pegoraro, and S. Sulis, "Improved Fine Particles Monitoring in Smart Cities by Means of Advanced Data Concentrator," *IEEE Transactions on Instrumentation and Measurement*, vol. 70, 2021, doi: 10.1109/TIM.2020.3031987.

[10] F. Pedersini, "Improving a Commodity Dust Sensor to Enable Particle Size Analysis," *IEEE Transactions on Instrumentation and Measurement*, vol. 68, no. 1, pp. 177–188, Jan. 2019, doi: 10.1109/TIM.2018.2834178.

[11] P. W. Oluwasanya, A. Alzahrani, V. Kumar, Y. A. Samad, and L. G. Occhipinti, "Portable multi-sensor air quality monitoring platform for personal exposure studies," *IEEE Instrumentation and Measurement Magazine*, vol. 22, no. 5, pp. 36–44, Oct. 2019, doi: 10.1109/IMM.2019.8868275.

[12] United States Environmental Protection Agency, "Sampling Methods for All Parameters | Air Quality System | US EPA," *AQS Reference Table*, Jul. 15, 2021. https://aqs.epa.gov/aqsweb/documents/codetables/methods_all.html (accessed Jul. 15, 2021).

[13] US EPA Office of Research and Development, "List of Designated Reference and Equivalent Methods (MD-D205-03)," Research Triangle Park, Jun. 2021. Accessed: Jul. 15, 2021. [Online]. Available: www.epa.gov/ttn/amtic/criteria.html

[14] J. P. Specht, S. Esfahani, Y. Xing, M. Cole, and J. W. Gardner, "Characterisation of Zinc Oxide Thin-Film Solidly Mounted Resonators for Particle Sensing in Air," in *2020 IEEE International Instrumentation and Measurement Technology Conference (I2MTC)*, May 2020, pp. 1–6. doi: 10.1109/I2MTC43012.2020.9129106.

[15] J. P. Black, A. Elium, R. M. White, M. G. Apte, L. A. Gundel, and R. Cambie, "MEMS-Enabled miniaturized particulate matter monitor employing 1.6 GHz aluminum nitride thin-film bulk acoustic wave resonator (FBAR) and thermophoretic precipitator," in *Proceedings - IEEE Ultrasonics Symposium*, 2007, pp. 476–479. doi: 10.1109/ULTSYM.2007.128.

[16] S. Thomas, F. H. Villa-López, J. Theunis, J. Peters, M. Cole, and J. W. Gardner, "Particle sensor using solidly mounted resonators," *IEEE Sensors Journal*, vol. 16, no. 8, pp. 2282–2289, 2016, doi: 10.1109/JSEN.2015.2512303.

[17] L. Djoumi, M. Vanotti, and V. Blondeau-Patissier, "Real time cascade impactor based on Surface Acoustic Wave delay lines for PM10 and PM2.5 mass concentration measurement," *Sensors (Switzerland)*, vol. 18, no. 1, p. 255, 2018, doi: 10.3390/s18010255.

[18] J. Sun, Z. Liu, K. Yang, and Y. Lu, "A miniature system for particulate matter (PM) measurement," in *2015 IEEE SENSORS*, Nov. 2015, pp. 1–4. doi: 10.1109/ICSENS.2015.7370246.

[19] S. Thomas, M. Cole, F. H. Villa-Lopez, J. W. Gardner, J. Peters, and J. Theunis, "A low-cost acoustic microsensor based system in package for air quality monitoring," *Proceedings of IEEE Sensors*, Jan. 2017, doi: 10.1109/ICSENS.2016.7808872.

[20] W. C. Hao, Z. Nie, J. L. Liu, M. H. Liu, and S. T. He, "Advances in a developed surface acoustic wave based particulate matter 2.5 monitor," in *Proceedings of the 2016 Symposium on Piezoelectricity, Acoustic Waves and Device Applications, SPAWDA 2016*, 2017, pp. 227–229. doi: 10.1109/SPAWDA.2016.7829993.

[21] M. Chellasivalingam, H. Imran, M. Pandit, A. M. Boies, and A. A. Seshia, "Weakly Coupled Piezoelectric MEMS Resonators for Aerosol Sensing," *Sensors*, vol. 20, no. 11, p. 3162, Jun. 2020, doi: 10.3390/S20113162.

[22] A. Fort, C. Trigona, E. Panzardi, V. Vignoli, T. Addabbo, and M. Mugnaini, "An AlN Micromachined Mass Sensor: Modeling and Characterization," *IEEE Transactions on Instrumentation and Measurement*, vol. 70, 2021, doi: 10.1109/TIM.2020.3008987.

[23] M. Bertke, I. Kirsch, E. Uhde, and E. Peiner, "Ultrafine Aerosol Particle Sizer Based on Piezoresistive Microcantilever Resonators with Integrated Air-Flow Channel," *Sensors*, vol. 21, no. 11, p. 3731, May 2021, doi: 10.3390/S21113731.

[24] A. Clements and R. Vanderpool, "FRMs/FEMs and Sensors: Complementary Approaches for Determining Ambient Air Quality.," in *EPA Tools and Resources Webinar*, Dec. 2019, p. 348237. Accessed: Oct. 09, 2021. [Online]. Available: https://www.epa.gov/sites/default/files/2019-12/documents/frm-fem_and_air_sensors_dec_2019_webinar_slides_508_compliant.pdf

[25] B. Giechaskiel *et al.*, "Review of motor vehicle particulate emissions sampling and measurement: From smoke and filter mass to particle number," *Journal of Aerosol Science*, vol. 67, pp. 48–86, 2014, doi: 10.1016/j.jaerosci.2013.09.003.

[26] A. R. Nosratabadi, P. Graff, H. Karlsson, A. G. Ljungman, and P. Leanderson, "Use of TEOM monitors for continuous long-term sampling of ambient particles for analysis of constituents and biological effects," *Air Quality, Atmosphere & Health*, vol. 12, no. 2, pp. 161–171, Nov. 2018, doi: 10.1007/S11869-018-0638-5.

[27] H. Zhou, Y. Song, X. Pan, and D. Li, "Airborne particles detection and sizing at single particle level by a novel electrical current pulse sensor," *Measurement*, vol. 92, pp. 58–62, Oct. 2016, doi: 10.1016/J.MEASUREMENT.2016.06.011.

[28] Y. Su, U. Sofowote, J. Debosz, L. White, and A. Munoz, "Multi-Year Continuous PM2.5 Measurements with the Federal Equivalent Method SHARP 5030 and Comparisons to Filter-Based and TEOM Measurements in Ontario, Canada," *Atmosphere*, vol. 9, no. 5, p. 191, May 2018, doi: 10.3390/ATMOS9050191.

[29] D. Schweizer, R. Cisneros, and G. Shaw, "A comparative analysis of temporary and permanent beta attenuation monitors: The importance of understanding data and equipment limitations when creating PM2.5 air quality health advisories," *Atmospheric Pollution Research*, vol. 7, no. 5, pp. 865–875, Sep. 2016, doi: 10.1016/J.APR.2016.02.003.

[30] N. Sang-Nourpour and J. S. Olfert, "Calibration of optical particle counters with an aerodynamic aerosol classifier," *Journal of Aerosol Science*, vol. 138, p. 105452, Dec. 2019, doi: 10.1016/J.JAEROSCI.2019.105452.

[31] R. Williams, A. Kaufman, T. Hanley, J. Rice, and S. Garvey, "Evaluation of Field-deployed Low Cost PM Sensors EPA/600/R-14/464," Washington DC, 2014. Accessed: Oct. 05, 2021. [Online]. Available: https://cfpub.epa.gov/si/si_public_record_report.cfm?Lab=NERL&dirEntryId=297517&simpleSearch=1&searchAll=EPA%2F600%2FR-14%2F464

[32] R. Williams *et al.*, "Performance Evaluation of the United Nations Environment Programme Air Quality Monitoring Unit EPA/600/R-17/171," Washington DC, Jul. 2017. Accessed: Oct. 05, 2021. [Online]. Available: https://cfpub.epa.gov/si/si_public_record_report.cfm?dirEntryId=336950&Lab=NERL

[33] J. P. Specht, S. Esfahani, M. Cole, and J. W. Gardner, "CMOS Compatible Aluminium Nitride Solidly Mounted Resonator with an Integrated Microheater for Temperature Modulation," in *2021 21st International Conference on Solid-State Sensors, Actuators and Microsystems (Transducers)*, Jun. 2021, pp. 1396–1399. doi: 10.1109/Transducers50396.2021.9495517.

[34] S. Thomas, M. Cole, F. H. Villa-López, and J. W. Gardner, "High frequency surface acoustic wave resonator-based sensor for particulate matter detection," *Sensors and Actuators, A: Physical*, vol. 244, pp. 138–145, 2016, doi: 10.1016/j.sna.2016.04.003.

[35] G. Sauerbrey, "Verwendung von Schwingquarzen zur Wägung dünner Schichten und zur Mikrowägung," *Zeitschrift für Physik*, vol. 155, no. 2, pp. 206–222, Apr. 1959, doi: 10.1007/BF01337937.

[36] G. Sauerbrey, "Verwendung von Schwingquarzen zur Wägung dünner Schichten und zur Mikrowägung,"

*Zeitschrift für Physik*, vol. 155, no. 2, pp. 206–222, Apr. 1959, doi: 10.1007/BF01337937.

[37] F. H. Villa-López, "CMOS compatible Solidly Mounted Resonator for air quality monitoring," Coventry, 2017. Accessed: Oct. 24, 2021. [Online]. Available: http://wrap.warwick.ac.uk/99931/

[38] F. H. Villa Lopez, M. Cole, E. Iborra, M. D. M. Ramos, and J. W. Gardner, "A Solidly Mounted Resonator With CMOS-Fabricated Acoustic Mirror For Low-Cost Air Quality Monitoring," in *2019 20th International Conference on Solid-State Sensors, Actuators and Microsystems and Eurosensors XXXIII, TRANSDUCERS 2019 and EUROSENSORS XXXIII*, Jun. 2019, pp. 1242–1245. doi: 10.1109/TRANSDUCERS.2019.8808790.

[39] E. Marigo *et al.*, "Monolithic BAW oscillator with conventional QFN packaging," in *IFCS/EFTF 2019 - Joint Conference of the IEEE International Frequency Control Symposium and European Frequency and Time Forum, Proceedings*, Apr. 2019, pp. 1–2. doi: 10.1109/FCS.2019.8855999.

[40] T. H. Tan, M. Soundara-Pandian, N. Shazwani, E. Marigo, R. A. Raj, and M. Subramaniam, "Evaluating Film Assisted Molding Packaging for Peizoelectric Micromachined Ultrasonic Transducers," in *Proceedings of the IEEE International Conference on Micro Electro Mechanical Systems (MEMS)*, Jan. 2021, vol. 2021-January, pp. 1044–1047. doi: 10.1109/MEMS51782.2021.9375366.

[41] Y. Liu, Y. Cai, Y. Zhang, A. Tovstopyat, S. Liu, and C. Sun, "Materials, Design, and Characteristics of Bulk Acoustic Wave Resonator: A Review," *Micromachines*, vol. 11, no. 7, p. 630, Jun. 2020, doi: 10.3390/mi11070630.

[42] R. J. Bruls, H. T. Hintzen, G. de With, and R. Metselaar, "The temperature dependence of the Young's modulus of MgSiN2, AlN and Si3N4," *Journal of the European Ceramic Society*, vol. 21, no. 3, pp. 263–268, Mar. 2001, doi: 10.1016/S0955-2219(00)00210-7.

**Jan Peter Specht** received an MEng degree in electronic engineering from the University of Warwick, UK, in 2018. He is currently pursuing a PhD degree in electronic engineering on film bulk acoustic resonators and their application as air quality sensors at the University of Warwick.

**Siavash Esfahani** received the MEng degree in electronic engineering from the University of Birmingham, UK, in 2012. He received the M.Sc. degree in electronic engineering with sensor technology and the Ph.D. degree from Warwick University, UK, in 2014 and 2018, respectively. His PhD dissertation was on Electronic Nose Instrumentation for Biomedical Applications. He is a Research Fellow at Warwick University, working on developing particle matter sensors using solid mount resonator sensors.

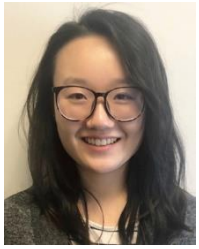

**Yuxin Xing** received a BEng degree and a PhD degree in electronic engineering from the University of Warwick, UK, in 2015 and 2020, respectively. She is currently a research fellow at the Microsensors and Bioelectronics Laboratory in the University of Warwick. Her research interest including different gas sensor technologies and their applications.

**Anton Köck** received his master's degree (1986) and Ph.D. (1989) in Experimental Physics at the University of Innsbruck, Austria. After a 4-years Post Doc position at the Walter Schottky Institute (TU Munich), he was at the Institute for Solid State Electronics (TU Vienna), where he habilitated in "Optoelectronics" in 1998. He was Professor for Physics and Material Science at the Wiener Neustadt University for Applied Sciences, then he was deputy head of the business unit "Nano Systems", Austrian Institute of Technology (AIT). Since 2013 he is Key Researcher at MCL and is head of the gas sensor research group. Major focus are advanced nanomaterials for chemical sensing, their integration on CMOS devices, and 3D-system integration. Anton Köck has more than 250 publications and conference contributions, has coordinated the FP7-project "MSP – Multi Sensor Platform for Smart Building Management" (Project No. 611887, FP7-ICT-2013-10), and has been the General Conference Chair of the EUROSENSORS 2018 conference.

**Marina Cole** received BSc degree from the University of Montenegro, (former Yugoslavia), and a Ph.D. degree from Coventry University, U.K. She was appointed to a lectureship in electronic engineering at Warwick University in 1998, promoted to associate professor in 2006, readership in 2017 and professorship in 2020. Her current research interests are in integrated silicon-based sensors, analogue, digital and mixed signal ASIC devices, smart sensors and microsystems. In particular, she is interested in development of CMOS based and CMOS compatible acoustic wave sensors for health and environmental monitoring especially particle sensing and VOC monitoring. Since 2001 she has been leading the work in the area of acoustic wave devices within the Microsensors & Bioelectronics Laboratory (MBL*)*. Professor Cole has published over 80 publications in scientific journals and conference proceedings. She is co-founder and Director of university spin-out company Sorex Sensors Ltd.

**Julian William Gardner** (F'18) obtained a first in physics from Birmingham University, followed by a PhD in physical electronics from Cambridge University and a DSc in Electronic Engineering from Warwick University. He has 5 years' experience in industry as an R & D Engineer and 30 years working in the field of chemical microsensors at Warwick University, and is currently Professor of Electronic Engineering. He founded several electronic nose companies in the 1990s. He co-founded Cambridge CMOS Sensors Ltd in 2008 with Florin Udrea and was its first CTO; in 2013 he became its Chief Scientist. His expertise is in the design of MEMS based chemical sensors, and the signal processing/data analysis of sensor arrays, including electronic noses and electronic tongues. He has published over 500 papers in the field of micro sensors, authored 10 books and over 25 patents. He has won various awards and medals from the IET, IEEE and Royal Society. He is also a Fellow of both the UK Institution of Engineering and Technology and the Royal Academy of Engineering.